

First Experimental Demonstration of 100 nm Inversion-mode InGaAs FinFET through Damage-free Sidewall Etching

Y.Q. Wu, R.S. Wang, T. Shen, J.J. Gu and P. D. Ye

School of Electrical and Computer Engineering and Birck Nanotechnology Center, Purdue University, West Lafayette, IN 47907, U.S.A.
Tel: 1-765-494-7611, Fax: 1-765-496-7443, Email: yep@purdue.edu

Abstract

The first well-behaved inversion-mode InGaAs FinFET with gate length down to 100 nm with ALD Al_2O_3 as gate dielectric has been demonstrated. Using a damage-free sidewall etching method, FinFETs with L_{ch} down to 100 nm and W_{Fin} down to 40 nm are fabricated and characterized. In contrast to the severe short-channel effect (SCE) of the planar InGaAs MOSFETs at similar gate lengths, FinFETs have much better electro-static control and show improved $S.S.$, $DIBL$ and V_T roll-off and less degradation at elevated temperatures. The SCE of III-V MOSFETs is greatly improved by the 3D structure design. The more accurate D_{it} estimation from the $S.S.$ is also presented.

Introduction

With the continuous request of carrier transport boosting in CMOS devices, very recently, much progress has been made on achieving on-state performance of inversion-mode In-rich InGaAs MOSFETs using high-k gate dielectrics [1-4]. However, the off-state performance of InGaAs MOSFETs is far from satisfactory according to ITRS requirement. The short-channel effect (SCE) of InGaAs MOSFETs deteriorates more quickly than Si MOSFETs due to its nature of narrower bandgap and higher semiconductor dielectric constant [5]. In order to achieve better gate control capability, new structure design like FinFET demonstrated successfully in Si devices [6-10], is strongly needed for short-channel III-V MOSFETs. However, unlike Si, the dry etching of III-V semiconductor surface has been believed to be difficult and uncontrollable [7], especially related with surface damage and integration with high-k dielectrics. In this paper, we report for the first experimental demonstration of inversion-mode $\text{In}_{0.53}\text{Ga}_{0.37}\text{As}$ tri-gate FinFET using damage-free etching and ALD Al_2O_3 as gate dielectric. The SCE is greatly suppressed in terms of subthreshold slope (SS), drain induced barrier lowering (DIBL) and threshold voltage (V_T) roll-off. Detailed analysis and comparison are performed on the FinFETs with channel length (L_{ch}) from 200 nm to 100 nm, fin width (W_{Fin}) from 100 nm to 40 nm, and fixed fin height (H_{Fin}) of 40 nm.

Experiments

Fig. 1 and Table 1 show the schematic cross section of the uniform device structure and the device fabrication flow. A 500 nm p-doped $2 \times 10^{18} \text{ cm}^{-3}$ InP layer, a 300 nm p-doped $2 \times 10^{16} \text{ cm}^{-3}$ and a 40 nm $2 \times 10^{16} \text{ cm}^{-3}$ $\text{In}_{0.53}\text{Ga}_{0.47}\text{As}$ channel layer were sequentially grown by MBE on a 2-inch InP p+ substrate. The

heavily doped InP layer beneath the channel was chosen to prevent punch through and reduce substrate leakage because of its higher bandgap. Due to the non-optimized source/drain junctions, the heavily doped InP layer resulted in worsen junction leakage. After surface degreasing and ammonia-based native oxide etching, the wafers were transferred via room ambient to an ASM F-120 ALD reactor. A 10 nm thick Al_2O_3 layer was deposited at a substrate temperature of 300°C as an encapsulation layer. Source and drain regions were selectively implanted with a Si dose of $1 \times 10^{14} \text{ cm}^{-2}$ at 20 keV through the 10 nm thick Al_2O_3 layer. The implantation condition was chosen carefully to achieve the desired junction depth and S/D doping concentration. Implantation activation was achieved by rapid thermal anneal (RTA) at 600 °C for 15 s in a nitrogen ambient. The reduction of activation temperature from 750 °C to 600 °C resulted in much improved S/D junction leakage while achieving similar activation efficiency. [5] A combined dry and wet etching was used to pattern the fin structures. HDPE BCl_3/Ar was used for dry etching while ZEP-520A electron-beam resist was used as a mask. A short dip of 3 seconds in diluted $\text{H}_2\text{SO}_4:\text{H}_2\text{O}_2:\text{H}_2\text{O}$ solution was carried out immediately after the dry etching to remove the damaged surface layer. The resulted fin channels have a depth of 40 nm which can be seen from the last SEM image in Fig. 3. More sophisticated process is needed to make the fin side-walls perfectly vertical. A 5 nm Al_2O_3 film was regrown by ALD after removing the encapsulation layer by BOE solution and $(\text{NH}_4)_2\text{S}$ surface preparation. After 400-500 °C PDA process, the source and drain ohmic contacts were made by an electron-beam evaporation of a combination of AuGe/Ni/Au and a lift-off process, followed by a RTA process at 320 °C for 30 s also in a N_2 ambient. The gate electrode was deposited by electron-beam evaporation of Ni/Au and a lift-off process. The fabricated MOSFETs have a nominal gate length varying from 100 nm to 150 nm and fin widths from 40 nm to 100 nm. The final 3D device structure is shown in Fig. 2. All patterns were defined by a Vistec VB-6 UHR electron-beam lithography (EBL) system. A Keithley 4200 was used for MOSFET output characteristics. The combined dry and wet etching for the formation of fin channels results in damage-free sidewalls. It is verified by the carrier transport through the fin channels without any significant degradation, compared to the planar devices.

Results and Discussions

Fig.4 shows the gate leakage current density (J_g) of 100 nm-long FinFET with W_{Fin} of 40 nm and 100 nm, compared to the planar device at $V_{\text{ds}}=0.8\text{V}$ on-state. The J_g of FinFETs

increases more than one order of magnitude but still remains in the range of 10^{-4} A/cm², which is about 8-9 orders of magnitude smaller than the drain current. The 3D structure would generally result in higher gate leakage current mostly from the corner regions, where electric field line is mostly crowded. Although ALD dielectric should be quite conformal, corner regions could also be the weakest point of dielectric strength. The small degradation suggests that the 5 nm Al₂O₃ is good enough for this 3D structure and leaves room for further EOT reduction. Fig. 5 shows the typical output characteristics of a planar 100 nm-long MOSFET. It cannot be turned off at zero gate bias due to the SCE [5]. Fig. 6 depicts the well-behaved output characteristic of a FinFET with 40 nm W_{Fin} at same channel length. From the comparison, it clearly shows the FinFET has much better behaved output characteristics in terms of off-state while maintaining the on-state performance. Fig. 7 shows the total channel resistance for FinFETs with three different channel lengths. The R_{sd} can be extracted to be $\sim 1200 \Omega \cdot \mu\text{m}$ as shown in the inset of Fig. 7.

Fig. 8 compares the transfer characteristics of a 100nm-long channel planar FET and FinFETs with W_{Fin} of 40 nm and 100 nm. The FinFETs have better off-state performance over the planar one. The 40 nm W_{Fin} device has the best electrostatic gate control of the channel. The on-off ratio of FinFETs improves almost by two orders of magnitude over the planar one. The positive V_{T} shift also suggests that the pinch-off characteristic for FinFET is better than the planar device. SS from the saturation region as well as DIBL are compared among FinFETs with 4 different W_{Fin} from 40 nm to 100 nm and the planar FET in Fig. 9 and Fig. 10. The trend shows the device with narrower W_{Fin} has better SS and DIBL as expected. The SS of FinFET with 100 nm channel length improves more than 34% percent and degrades much slower when channel length gets shorter. The DIBL is greatly reduced from 440 mV/V for the planar device to 180 mV/V for the FinFET at 100 nm gate length. Fig. 11 and Fig. 12 show the relation of SS and DIBL with the ratio of $W_{\text{Fin}}/L_{\text{ch}}$. Both SS and DIBL is roughly proportional to $W_{\text{Fin}}/L_{\text{ch}}$. It shows that further channel length scaling can be achieved by narrowing the fin width to avoid SCE. V_{T} roll-off, another important metric for SCE is shown and compared in Fig. 13 among planar device, 40 nm W_{Fin} and 100 nm W_{Fin} devices, all with 100 nm channel length. V_{T} is determined by 1 $\mu\text{A}/\mu\text{m}$ metrics at $V_{\text{ds}}=0.8\text{V}$. The 40 nm W_{Fin} FinFET shows smallest V_{T} roll-off, which is only 30% of the planar FET and the degradation of V_{T} roll-off when channel length gets shorter is smaller compared with the planar FET.

At elevated ambient temperatures, Fig. 14 and Fig. 15 compare SS of the three FETs at $V_{\text{ds}}=0.05\text{V}$ and $V_{\text{ds}}=0.8\text{V}$, respectively. The FinFETs have much better SS at varying temperatures. The fact that the channel surfaces of FinFET should be not better than the planar devices, if not worse after going through all the patterning and etching processes. It is clear that the SS is not only affected by interface trap density, but also by SCE. Simple estimation of interface trap density (D_{it}) from SS would result in gross overestimation of D_{it} . At the

linear region, SS of FinFETs in Fig. 15 are lower than those from the planar FET, indicating that the interface properties of Al₂O₃/InGaAs on the etched sidewalls are not degraded much by the fin etching process, or D_{it} on the sidewalls is not much larger than that on the planar structures. It verifies that the newly developed dry/wet etching process is *damage-free* and suitable for 3D III-V device fabrication. Fig. 16 and Fig. 17 show DIBL and V_{T} roll-off of the three FETs at different temperatures. Unlike SS with strong dependence of D_{it} , DIBL and V_{T} roll-off clearly show that FinFETs offer much better tolerance at raised temperatures. DIBL and V_{T} of FinFETs with $W_{\text{Fin}}=40$ nm changed 60 mV/V and 0.2 V, compared to 175 mV/V and 0.48 V of the planar FET. Although D_{it} can be simply estimated from SS at linear region in long-channel devices, it's also possible to estimate the D_{it} value by counting the SCE in short-channel devices. SS is found to be proportional with the ratio $W_{\text{Fin}}/L_{\text{ch}}$ from the experimental data as shown in Fig. 18. When $W_{\text{Fin}}/L_{\text{ch}} \rightarrow 0$, SCE is eliminated since the best electro-static control of the channel is achieved with the thinnest fin. By taking extrapolated SS at $W_{\text{Fin}}/L_{\text{ch}}=0$, more intrinsic SS can be obtained and used to estimate D_{it} for deep-submicron InGaAs FinFETs. The upper limit of average D_{it} on the top and sidewall surfaces in In_{0.53}Ga_{0.47}As FinFET is $1.7 \times 10^{12}/\text{cm}^2\text{-eV}$ from the data in Fig. 18. The similar trend is also observed from the simple calculation of SS vs. $W_{\text{Fin}}/L_{\text{ch}}$ as a function of D_{it} . The result confirms that the newly developed dry/wet etching process produces damage-free InGaAs sidewalls and the high-k/3D InGaAs interface is comparable to the 2D case.

Conclusion

We have demonstrated the first well-behaved inversion-mode InGaAs FinFET with ALD Al₂O₃ as gate dielectric. Detailed analysis of SS, DIBL and V_{T} roll-off are carried out on FinFETs with L_{ch} down to 100 nm and W_{Fin} down to 40 nm. The SCE of planar InGaAs MOSFETs is greatly improved by the 3D structure design.

Acknowledgement

The authors would like to thank D.A. Antoniadis, M.S. Lundstrom, and J. del Alamo for the valuable discussions. The work is supported in part by NSF, the SRC FCRP MSD Focus Center and DoD Army Research Office.

References

- [1] Y. Xuan et al., *IEEE Electron Device Lett.*, **29**, 294 (2008).
- [2] T.D. Lin et al. *Applied Physics Letters* **93**, 033516 (2008).
- [3] N. Goel et al., *IEDM Tech. Dig.* 363 (2008).
- [4] Y. Sun et al., *IEDM Tech. Dig.* 367 (2008).
- [5] Y.Q. Wu et al., *IEEE Electron Device Lett.*, **30**, 700 (2009).
- [6] D. Hisamoto et al., *IEEE Trans. Electron Device*, **47**, 2320 (2000).
- [7] H.-S.P Wong, *IBM J. Res. & Dev.* **46**, 133 (2002).
- [8] B.S. Doyle et al., *IEEE Electron Device Lett.*, **24**, 263 (2003).
- [9] A. Veloso et al., *IEDM Tech. Dig.* 861 (2008).
- [10] J.-W. Yang et al., *VLSI Tech. Dig.* 20 (2008).

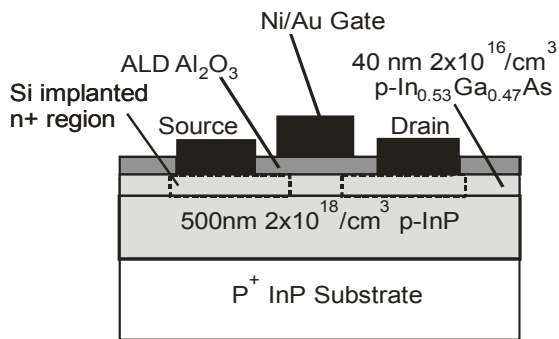


Fig. 1 Schematic cross-section view of an inversion-mode planar n-channel $\text{In}_{0.53}\text{Ga}_{0.47}\text{As}$ ($2 \times 10^{16}/\text{cm}^3$) MOSFET with 5nm ALD Al_2O_3 as gate dielectric. A heavily doped wide bandgap InP lies underneath the channel.

- 1) NH_4OH surface treatment and ALD Al_2O_3 10nm deposition
- 2) S/D patterning and Si implantation ($20\text{KeV} / 1 \times 10^{14}/\text{cm}^2$)
- 3) Si implanted S/D activation using RTA (600°C 15s in N_2)
- 4) Fin patterning, dry etching by HDPE BCl_3/Ar using ZEP resist as mask and 3 sec dip in very diluted $\text{H}_2\text{SO}_4:\text{H}_2\text{O}_2:\text{H}_2\text{O}$ solution
- 5) $(\text{NH}_4)_2\text{S}$ treatment 5nm ALD re-growth
- 6) PDA: $400\text{-}500^\circ\text{C}$ 30s in N_2
- 7) S/D contact patterning and Au/Ge/Ni ohmic metal and 320°C anneal
- 8) Gate patterning, Ni/Au evaporation and lift-off

Table 1 Fabrication process flow for inversion-mode high-k/InGaAs FinFETs. 10 nm Al_2O_3 acts as an encapsulation layer to protect the surface during implantation and the following activation. All patterns were defined by a Vistec VB-6 UHR electron beam lithography system. Dry etching was done by Panasonic E620 high density plasma etcher (HDPE).

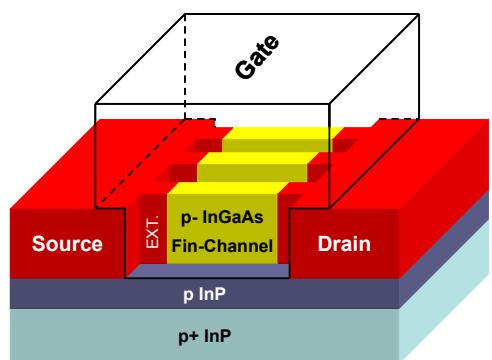


Fig. 2 Three-dimensional schematic view of the $\text{In}_{0.53}\text{Ga}_{0.47}\text{As}$ FinFET (5 nm Al_2O_3 is conformally deposited on fin-channels and not shown here). Non-self-aligned structure was used with the gate overlapping part of the implanted source and drain. The non-self-aligned structure provides better source/drain access resistance at the extension regions.

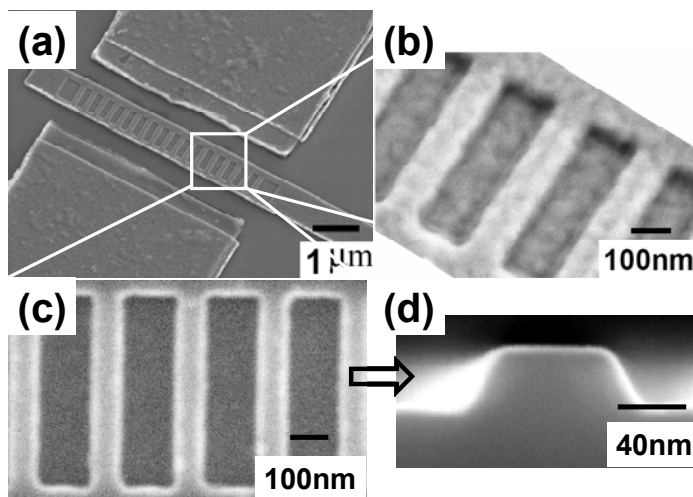


Fig.3 (a) Tilted SEM image of a finished FinFET device. (b) Zoomed-in image of the channel region covered with gate dielectric and gate metal. (c) SEM image of the fin structure after dry etching. (d) Cross section SEM image of a fin after dry etching.

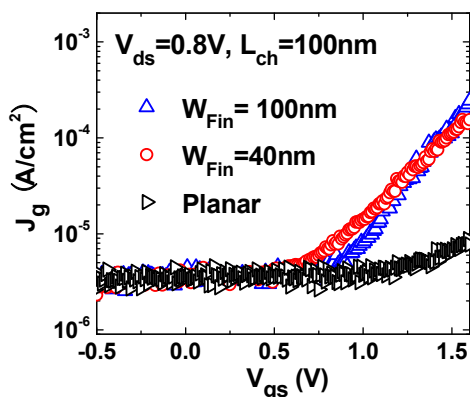


Fig. 4 Gate leakage current through 5nm ALD Al_2O_3 gate dielectric of the planar FET and FinFETs with two fin widths. The leakage current of FinFETs increases around $2 \times 10^{-4} \text{A}/\text{cm}^2$ at $V_{\text{gs}}=1.6\text{V}$ and $V_{\text{ds}}=0.8\text{V}$.

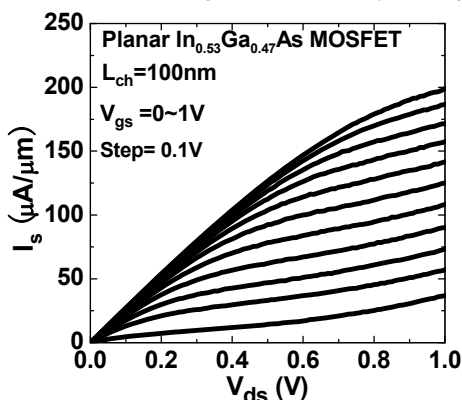


Fig.5 I_s vs V_{ds} of a planar MOSFET with $L_{\text{ch}}=100 \text{nm}$. The channel cannot be pinched off at zero gate bias due to the severe SCE [5].

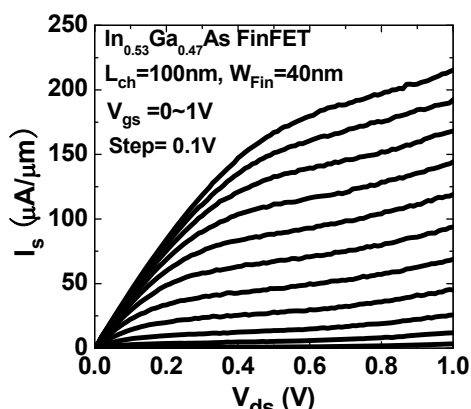


Fig.6 I_s vs V_{ds} of a FinFET device with $L_{\text{ch}}=100\text{nm}$ and $W_{\text{Fin}}=40\text{nm}$. The channel is much better pinched off compared to Fig. 5. I_{ds} is normalized by $W_{\text{Fin}}+2H_{\text{Fin}}$.

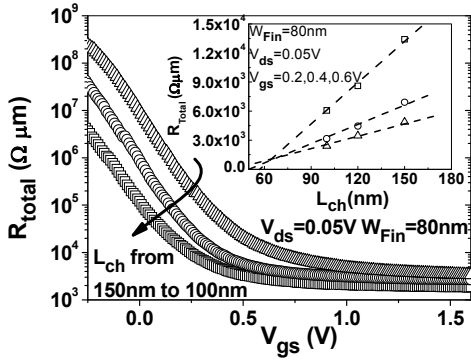


Fig. 7 R_{total} of $W_{fin}=80\text{nm}$ FinFETs with three different channel lengths from 150nm to 100nm. Inset: R_{sd} can be extracted around $1200\ \Omega\cdot\mu\text{m}$.

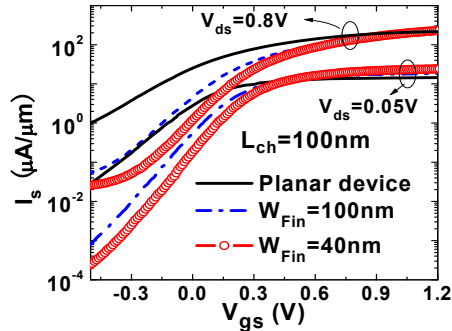


Fig. 8 Transfer characteristics of FinFETs and planar FET. Better electrostatic control of FinFETs reduces the SCE.

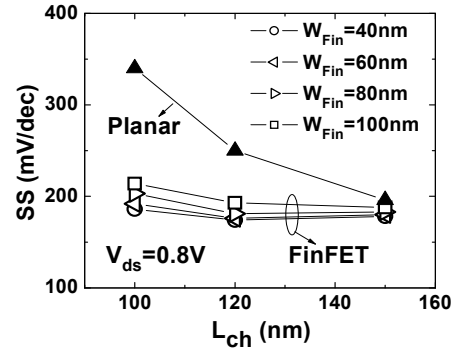


Fig. 9 Comparison of SS of FinFETs and planar FET. SS is greatly improved for the FinFETs.

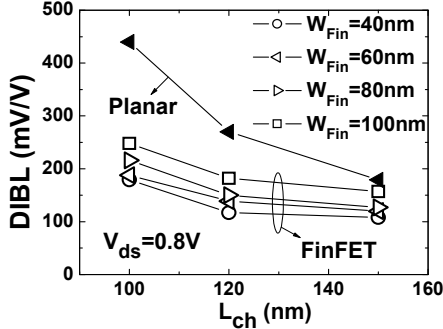


Fig. 10 Comparison of DIBL of FinFETs and planar FET.

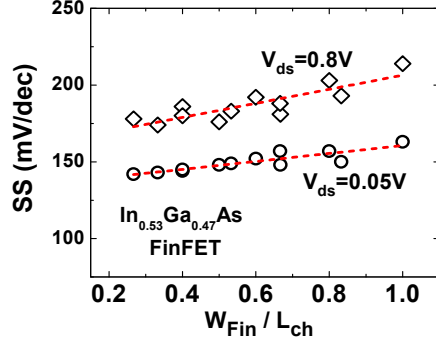


Fig. 11 SS vs W_{Fin}/L_{ch} at both linear region and saturation region.

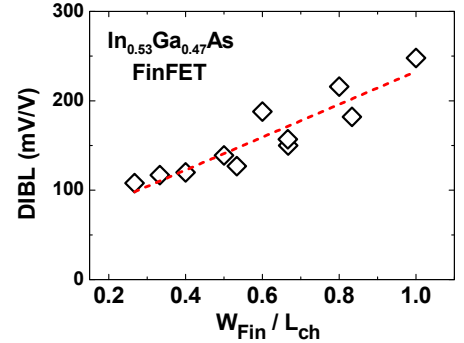


Fig. 12 DIBL vs W_{Fin}/L_{ch} for the FinFET.

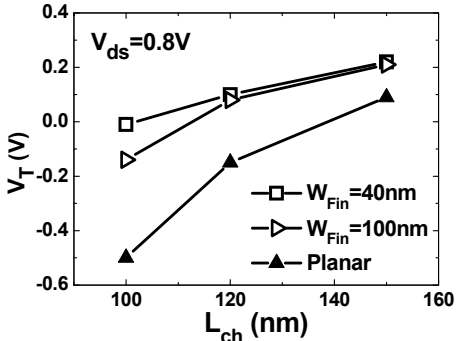


Fig. 13 Saturation V_T roll-off of planar FET is suppressed by FinFETs with different W_{Fin} .

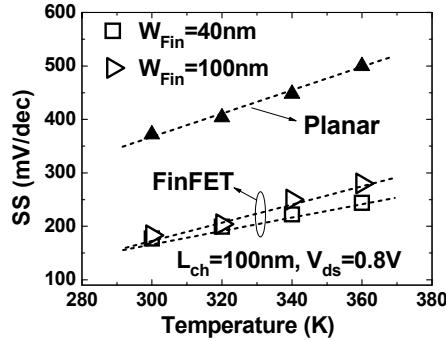


Fig. 14 Comparison of SS of planar FET and FinFETs at raised temperatures at $V_{ds}=0.8\text{V}$.

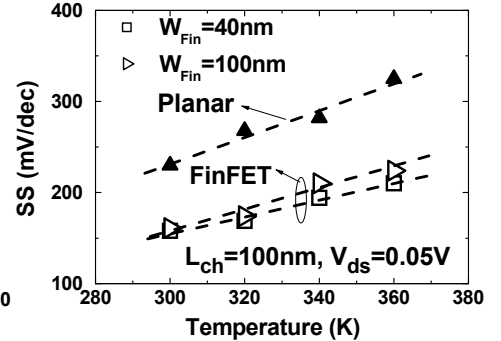


Fig. 15 Comparison of SS of planar FET and FinFETs at raised temperatures at $V_{ds}=0.05\text{V}$.

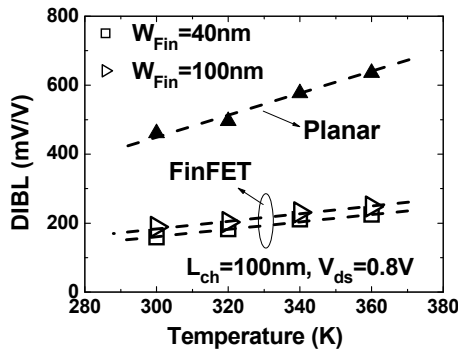


Fig. 16 Comparison of DIBL of planar FET and FinFETs at raised temperatures.

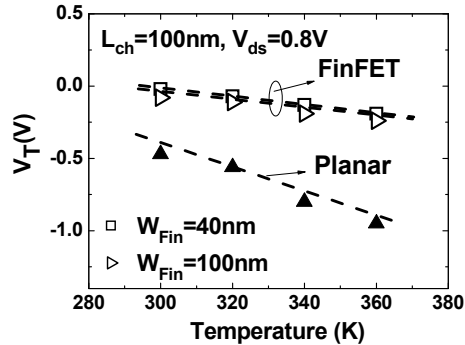


Fig. 17 Comparison of V_T roll-off of planar FET and FinFETs at raised temperatures.

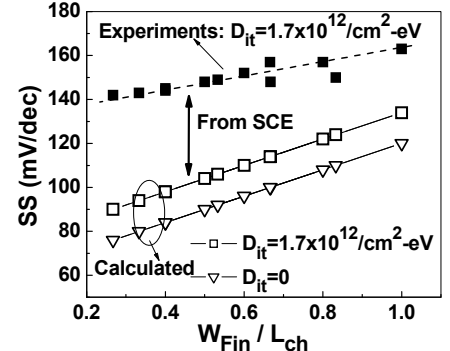


Fig. 18 Calculated SS vs W_{Fin}/L_{ch} w/o SCE, which reflects the real SS degradation on D_{it} . The vertical shift between calculated values and the experimental values is due to the SCE.